AIP | Journal of Applied Physics

Thermal transport in thin films measured by time-resolved, grazing incidence x-ray diffraction

D. A. Walko, Y.-M. Sheu, M. Trigo, and D. A. Reis

Citation: J. Appl. Phys. **110**, 102203 (2011); doi: 10.1063/1.3661164
View online: http://dx.doi.org/10.1063/1.3661164
View Table of Contents: http://jap.aip.org/resource/1/JAPIAU/v110/i10
Published by the AIP Publishing LLC.

Thermal transport in thin films measured by time-resolved, grazing incidence x-ray diffraction

D. A. Walko,[1,a)] Y.-M. Sheu,[2] M. Trigo,[3,4] and D. A. Reis[3,4]
[1]*Advanced Photon Source, Argonne National Laboratory, Argonne, Illinois 60439, USA*
[2]*FOCUS Center and Department of Physics, University of Michigan, Ann Arbor, Michigan 48109, USA*
[3]*PULSE Institute, SLAC National Accelerator Laboratory, Menlo Park, California 94025, USA*
[4]*Departments of Photon Science and Applied Physics, Stanford University, Stanford, California 94305, USA*

(Received 15 October 2010; accepted 6 March 2011; published online 30 November 2011)

We use depth- and time-resolved x-ray diffraction to study thermal transport across single crystal Bi films grown on sapphire in order to determine the thermal conductivity of the film and the Kapitza conductance of the interface. Ultrafast Ti:sapphire laser pulses were used to heat the films; x-ray diffraction then measured the film's lattice expansion. Use of grazing incidence diffraction geometry provided depth sensitivity, as the x-ray angle of incidence was varied near the critical angle. The shift of the film's Bragg peak position with time was used to determine the film temperature averaged over an x-ray penetration depth that could be selected by choice of the angle of incidence. For films that were thick compared to the laser penetration depth, we observed a large temperature gradient at early times. In this case, measurements with the incident angle near or well above the critical angle were more sensitive to the film conductivity or Kapitza conductance, respectively. For thinner films, however, cooling was dominated by the Kapitza conductance at all accessible time scales. © *2011 American Institute of Physics*. [doi:10.1063/1.3661164]

I. INTRODUCTION

With the continuing drive in nanotechnology to shrink electronic and electro-optical devices, temperature control and heat dissipation have become increasingly critical to the design and use of such devices.[1,2] Time-resolved x-ray diffraction (TRXD), using an ultrafast laser as a heat source in a pump-probe experiment, is a well-established noncontact method of measuring thermal transport in micro- and nanostructured systems. Due to the relatively weak interaction of x-rays with matter, TRXD has been applied to probe temperature changes of buried layers.[3–6] In a specular diffraction geometry for, say, a metal film, the penetration depth of x-rays is typically on the μm scale, while the optical absorption length may be only tens of nm. Typically, the long penetration depth of x-rays is considered an advantage. However, this mismatch between the penetration depths of the pump and probe also means that the x-rays may average across a significant temperature gradient, extending into the depth of the sample. For sufficiently perfect crystals, the temperature gradient may be calculated from the detailed shape of the x-ray rocking curve via fits using Takagi-Taupin theory,[7–9] or uniformity of temperature can be attempted with a thin-film sample, whose thickness is comparable to the lesser of the pump or probe attenuation lengths.

In this work, we perform depth-sensitive TRXD on thin films whose thickness D is substantially greater than the laser penetration depth λ_L but less than the x-ray linear attenuation length.[10] Using grazing-incidence (GI) x-ray diffraction, we limit the x-ray penetration depth λ_x by selecting an x-ray angle of incidence α near the critical angle for external reflection, α_c. Using $1-\delta-i\beta$ for the material's index of refraction and Λ as the x-ray wavelength, the critical angle $\alpha_c=\sqrt{2\delta}$. The x-ray penetration depth is therefore[11]

$$\lambda_x=\frac{\sqrt{2}}{4\pi}\Lambda[((\alpha^2-\alpha_c^2)^2+4\beta^2)^{1/2}+\alpha_c^2-\alpha^2]^{-1/2}. \quad (1)$$

To demonstrate the GI-TRXD technique, we choose thin films of Bi grown on sapphire. Achieving depth sensitivity through grazing incidence is, certainly, a well-established technique. GI-TRXD was first demonstrated for femtosecond phonon dynamics in Bi by Johnson *et al.*[12,13] Previously, we compared this method of determining thermal transport properties to use of the specular Bragg peak;[14] in this paper, we focus our analysis on the grazing incidence technique only and compare the results on two samples whose only nominal difference is in film thickness. Specifically, we will describe how to determine κ and σ_K, the thermal conductivity of the film and the Kapitza conductance of the interface, respectively, by performing TRXD at several angles of incidence.

II. EXPERIMENTAL DETAILS

These measurements were performed at insertion device beamline 7ID of the advanced photon source.[15] 7-keV x-rays were selected by a diamond (111) double-crystal monochromator and delivered to the sample mounted on a six-circle diffractometer. A Rh-coated mirror focused the x-rays horizontally to a width <100 μm. For each sample, measurements were repeated at several values of α, the angle of incidence, in order to vary the x-ray penetration into the film.

Diffracted x-rays were detected with an avalanche photodiode (APD) in photon-counting mode. The temporal response of the APD was fast enough to isolate individual

a)Electronic mail: d-walko@anl.gov.

x-ray bunches arriving at a 6.5 MHz rate. Electronic gating selected the specific bunch, which was coincident with the laser arrival at the sample (providing what we refer to as the "laser on" signal) as well as the same bunch one round trip earlier ("laser off"). Dead-time corrections were used to correct the observed count rate.[16] The laser used for heating the films was an amplified Ti:sapphire laser operating at a 5 kHz repetition rate. The laser pulses were centered at 800 nm with a ~50 fs pulse duration. A laser fluence of approximately 0.2 mJ/cm^2 was absorbed in the films. The laser beam was *not* in grazing incidence; rather, the angle of incidence was ~20° from normal. In this configuration, the laser penetration depth $\lambda_L \sim 15$ nm, based on the optical properties of Bi at 800 nm.

Two Bi films were grown by molecular-beam epitaxy on $1 \times 1\,\text{cm}^2$ c-axis sapphire substrates for these measurements. The films are single crystals with the c axis (the trigonal axis) perpendicular to the surface. In this paper, we index the diffraction spots in a hexagonal representation. For 7-keV x-rays, $\alpha_c = 0.43°$. Following Eq. (1), for $\alpha = 0.4°$ and 3.0°, the nominal x-ray penetration depth λ_x is 3.6 and 159 nm, respectively, assuming an ideally smooth surface. The first sample, which we refer to as the thin film, is 65 nm thick; the other, the thick film, is 284 nm thick. The thickness of the thinner film was measured by low-angle x-ray reflectivity; for the thicker film, the thickness was measured by optical (laser) pump-probe acoustic echoes. The miscuts of the films, as measured using optical reflectivity to determine the optical surface normals, were $< 0.5°$. The full widths of the 006 Bragg peaks were 0.23° for the thinner film and 0.54° for the thicker film, suggesting a higher crystalline quality (i.e., lower mosaic spread) for the thinner film. Figure 1 shows 014 rocking curves from each of the two samples. The two curves for each sample are the laser-on and laser-off data. The diffraction peaks in Fig. 1 are scanned along the out-of-plane reciprocal lattice coordinate L, rather than radially in a theta/two-theta scan. The in-plane lattice parameters of the film are constrained by the substrate, so all lattice expansion is along the c axis.

In these GI measurements, the signal from the Bi films is relatively weak compared to standard TRXD scattering geometries, especially at the smallest angles. Along with the dependence of λ_x on α (Eq. (1)), the x-ray footprint eventually becomes larger than the length of the sample at small enough α. Data collection rates are further limited by the 5 kHz repetition rate of the laser. Therefore, to achieve reasonable signal-to-noise ratios in the limited beamtime available, we measured the laser-on and laser-off signals at one point on the high-angle side of the 014 diffraction peak ($L = 4.02$ reciprocal lattice units, as indicated in Fig. 1). Depending on α, count times from 30 up to 240 s per point were necessary for acquisition of good counting statistics. For a Gaussian-shaped peak with small position shifts in L, the change in intensity on the side of the film's diffraction peak has been shown to be proportional to the shift of the peak and, thus, to the temperature change of the film.[3] For convenience in comparing data from different grazing angles, we plot the normalized difference of laser on and laser off in the upcoming figures. The calculated temperatures are plotted on the same axes by scaling the calculations to the data at late times (>5 ns for the thin film, >40 ns for the thick film); effectively, this treats the absorbed laser fluence, a quantity which is relatively difficult-to-measure, as a free parameter.

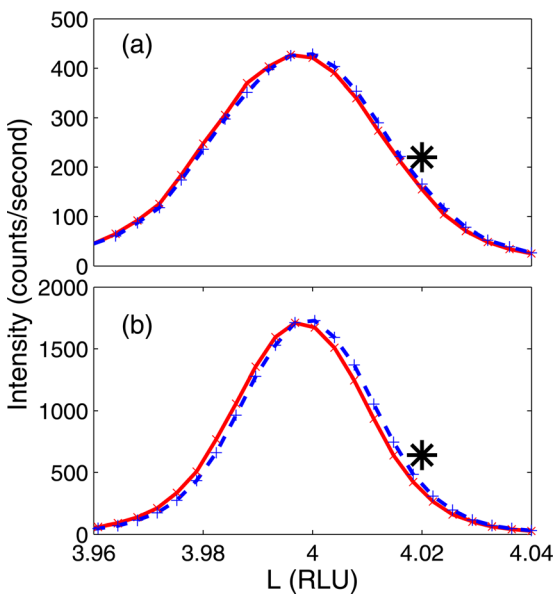

FIG. 1. (Color online) Time-resolved Bragg diffraction peaks in grazing geometry of the 014 reflections of (a) a 65-nm Bi film and (b) a 284-nm Bi film. The dashed (blue) lines show the rocking curves before laser excitation ("laser off"). The solid (red) lines show the rocking curves displaced to lower angle shortly after laser excitation ("laser on"). The laser/x-ray delays for the thin and thick films are 2.3 ns and 250 ps, respectively. The large star symbols mark the location of GI-TRXD data collected in Figs. 2 and 3.

III. RESULTS

Our GI-TRXD data are shown in Figs. 2 and 3. For the thinner film, measurements were made at $\alpha = 0.5°$ and 3.0°, with corresponding x-ray penetration depths of $\lambda_x = 11.8$ nm and 159 nm. While data from the shallower angle is more surface-sensitive and data from the higher angle is a nearly uniform average over the depth of the film, the measured

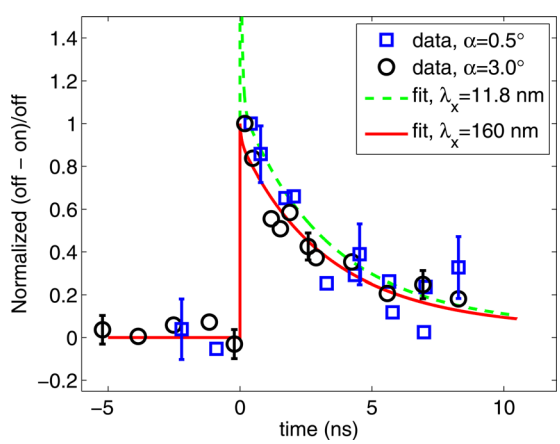

FIG. 2. (Color online) Normalized difference between the laser-off and laser-on signals, as gated by the APD detector, for the thin Bi film (65 nm). Symbols display the data (with selected error bars representing uncertainty due to counting statistics) and lines display best fits according to Eqs. (2)–(4). The angles of incidence and effective x-ray penetration depths are as listed in the legend.

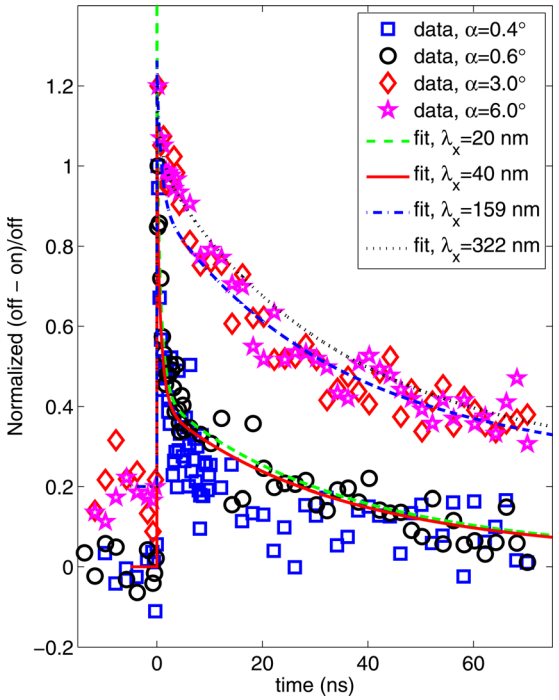

FIG. 3. (Color online) Data and fit for the thick Bi film (284 nm). Results for the higher two angles are offset vertically for clarity.

decay curves track fairly closely as the temperature of the film quickly becomes uniform. Simple fits to an exponential decay give time constants of 4 to 5 ns. For the thicker film, measurements were made at $\alpha = 0.4°$, 0.6°, 3.0°, and 6.0°. The data from the shallower angles exhibit a faster decay, indicative of heat dissipating away from the very top of the film. Fitted time constants over the whole range of measurement were ~30 ns, but fits to the early times gave time constants shorter than 10 ns. Data from the larger angles tend to decay more slowly (time constants ~40 ns), reflecting the cooling of the whole film by heat transfer into the substrate.

For a quantitative analysis of our data, we numerically solve the one-dimensional thermal diffusion equation for both the film and substrate,

$$\frac{dT(t,x)}{dt} = (\kappa/C)\frac{d^2T(t)}{dz^2}, \tag{2}$$

where T, C, and κ are the temperature rise, heat capacity, and lattice thermal conductivity. For the sapphire substrate, we use 3.1 J/cm^3/K for the specific heat and 34.8 W/m/K for the thermal conductivity. For the film, we assume a specific heat of 1.19 J/cm^3/K. The boundary condition at the interface ($z = D$) is

$$C\frac{dT(t)}{dt} = -\sigma_K \frac{dT}{dz}|_{z=D}, \tag{3}$$

where σ_K is the Kapitza (boundary) conductance. Finite values of this parameter give rise to a temperature differential at the interface; various models have been constructed to connect σ_K to the probability of phonon transmission across the interface. At the top surface of the film ($z = 0$), we use the insulating boundary condition

$$\frac{dT}{dz}|_{z=0} = 0. \tag{4}$$

We use, as an initial temperature profile in the film, $T(0 < z < D,\ t = 0) = T_0 \exp(-z/\lambda_L)$. T_0 is the initial maximum temperature rise, which could be on the order of 10 s of K if the assumed exponential form is correct. To compare with a data set collected at a given α, an average film temperature is calculated, weighted by an exponential factor with appropriate length scale λ_x. The best fit for Kapitza conductance across the Bi/sapphire interface is 2500 ± 100 W/cm^2/K from the thin film; data from this film is insensitive to κ. More specifically, as we show below, this film is sensitive to κ only for the first ~100 ps. For the thick film, the measured Kapitza conductance is 1100 ± 150 W/cm^2/K. The film's thermal conductivity is 10 ± 3 J/m/K. However, we note that the best fit occurs with $\lambda_L = 50$ nm. This value for the laser penetration depth is several times greater than expected from published optical constants, but includes the effect of fast electron transport on the initial temperature profile.

IV. DISCUSSION AND OUTLOOK

To summarize, we have used GI-TRXD to study thermal transport properties in thin films of Bi on $\alpha - Al_2O_3$. The film's thermal conductivity, which could only be measured from the thicker sample, is consistent with published values of 8 J/m/K for Bi; the strong correlation of thermal transport with other parameters in the calculation make a more exact determination difficult with this method. The measured values of σ_K for the two films are quite different. The best fit for the thicker film, but not the thinner film, is roughly consistent with the value of σ_K expected from the basic radiation limit model. As described elsewhere,[14] in this limiting case, phonons of all frequencies can cross the interface up to the lower cut-off frequency of the two materials. Based on the Debye temperature of Bi, the cutoff frequency is 2.5 THz; this yields a Kapitza conductance of $\sigma_K = 1300$ W/cm^2/K. Instead, use of 2.93 THz for bismuth's Raman-active A_{1g} phonon yields $\sigma_K = 2060$ W/cm^2/K. This value is closer to the result from the thin sample, a higher quality crystal whose cooling is dominated by σ_K on all accessible time scales. This result, we argue, better reflects the fundamental value of σ_K; the lower value observed for the thicker film appears to be a result of a lower quality interface.

The noncontact method we describe should be generally applicable to determination of thermal properties in thin films and multilayer structures. It provides tunable depth dependence as well as the ability to directly access the temperature of subsurface crystalline material. The sensitivity of these measurements to the parameters of interest depends on the time scales accessible to experiment. We define the sensitivity (see., e.g., Ref. 17) of measured value X to parameter ξ as a log differential in the form

$$S_\xi = \frac{\partial \ln(X)}{\partial \ln(\xi)}. \tag{5}$$

In Fig. 4, we plot S_{σ_K} and S_κ for the two films with two values of α each (0.5° and 3.0°), where X from Eq. (5) is the

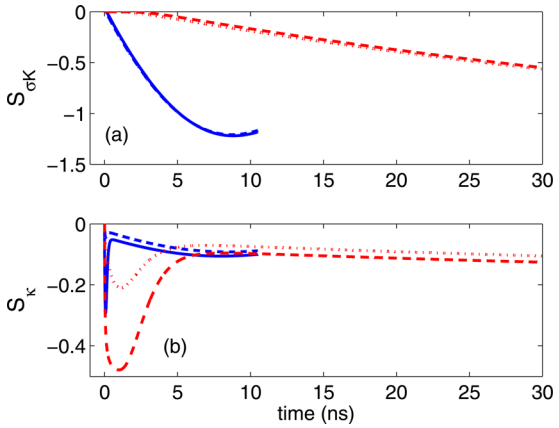

FIG. 4. (Color online) Sensitivity parameters, as defined in Eq. (5), for (a) the Kapitza conductance and (b) the film's thermal conductivity vs time. The solid and dash-dot lines represent the sensitivity for the 65-nm Bi film at $\alpha = 0.5°$ and 3.0°, respectively. The dashed and dotted lines represent the same grazing angles, respectively, for the 248-nm Bi film.

time-dependent temperature averaging over a depth of $\lambda_x = 11.8$ or 159 nm. After a short delay, the Kapitza conductance clearly dominates the temperature profile of either film, with little if any dependence on grazing angle. On the other hand, the measurements are fairly insensitive to the film's thermal conductivity, except at early times. The thinner film is sensitive to κ only for the more grazing angle and only for the first ~100 ps, which is comparable to the minimum time scale accessible in the present measurements (limited by the x-ray bunch duration). The thicker film is sensitive to κ for several ns and, over this time scale, enhanced at grazing incidence. Thus, the choice of film thickness (thicker or thinner) for these measurements can be guided by the preference in parameter of interest (σ_K or κ, respectively).

The long x-ray footprints at grazing incidence will generally require a laterally uniform sample as well as laterally uniform illumination by the pump laser. Nevertheless, as a diffraction-based technique, GI-TRXD may, in principle, be applicable to a laterally structured surface if materials in the areas of interest have strong diffraction peaks that can be clearly resolved from those of other materials in the illuminated volume. Count rates may also suffer if the signal comes from only a small area of the sample surface; a high-brightness x-ray source is necessary for these experiments. A high repetition rate for the pump laser will also improve the data-collection rate.

We note that fits to the lower- α data sets for the thicker film are slightly improved by averaging over a larger depth than expected from Eq. (1) for the given angle α. Empirically, we find better fits for the $\alpha = 0.4°$ and 0.6° data to be with $\lambda_x = 15$ nm and 40 nm, respectively, rather than the nominal 3.6 nm and 21 nm expected for a flat sample surface. This discrepancy could be due to an angular misalignment on the order of ~0.1° or a ~1 nm rms surface roughness; either would increase the depth of material being probed. Also conceivable is that the focusing mirror could induce a horizontal divergence that would cause a spread in α, even causing some portion of the x-ray beam to be incident at angles greater than the critical angle. However, in the present setup, the divergence due to the mirror is ~0.03° and thus should not be an appreciable factor here. To avoid this complication in the future, an energy-resolving detector can be used to measure the x-ray fluorescence of the film, providing an independent means of determining the volume of material being illuminated.

ACKNOWLEDGMENTS

We thank Ctirad Uher for providing the samples used in this work. Use of the APS was supported by the U.S. Department of Energy, Office of Science, Office of Basic Energy Sciences under Contract. No. DE-AC02-06CH11357. This work was supported in part by the U.S. DOE Grants No. DE-FG02-00ER1503 and from the NSF FOCUS physics frontier center.

[1]D. G. Cahill, W. K. Ford, K. E. Goodson, G. D. Mahan, A. Majumdar, H. J. Maris, R. Merlin, and S. R. Phillpot, J. Appl. Phys. **93**, 793 (2003).
[2]W. S. Capinski, H. J. Maris, T. Ruf, M. Cardona, K. Ploog, and D. S. Katzer, Phys. Rev. B **59**, 8105 (1999).
[3]M. Highland, B. C. Gundrum, Y. K. Koh, R. S. Averback, D. G. Cahill, V. C. Elarde, J. J. Coleman, D. A. Walko, and E. C. Landahl, Phys. Rev. B **76**, 075337 (2007).
[4]Y. M. Sheu, S. H. Lee, J. K. Wahlstrand, D. A. Walko, E. C. Landahl, D. A. Arms, M. Reason, R. S. Goldman, and D. A. Reis, Phys. Rev. B **78**, 045317 (2008).
[5]S. H. Lee, A. L. Cavalieri, D. M. Fritz, M. C. Swan, R. S. Hegde, M. Reason, R. S. Goldman, and D. A. Reis, Phys. Rev. Lett. **95**, 246104 (2005).
[6]M. Trigo, Y. M. Sheu, D. A. Arms, J. Chen, S. Ghimire, R. S. Goldman, E. Landahl, R. Merlin, E. Peterson, M. Reason, and D. A. Reis, Phys. Rev. Lett. **101**, 025505 (2008).
[7]C. R. Wie, T. A. Tombrello, and T. Vreeland, Jr., J. Appl. Phys. **59**, 3743 (1986).
[8]C. Rose-Petruck, R. Jimenez, T. Guo, A. Cavalleri, C. W. Siders, F. Raksi, J. A. Squier, B. C. Walker, K. R. Wilson, and C. P. J. Barty, Nature **398**, 310 (1999).
[9]A. M. Lindenberg, I. Kang, S. L. Johnson, T. Missalla, P. A. Heimann, Z. Chang, J. Larsson, P. H. Bucksbaum, H. C. Kapteyn, H. A. Padmore, R. W. Lee, J. S. Wark, and R. W. Falcone, Phys. Rev. Lett. **84**, 111 (2000).
[10]B. L. Henke, E. M. Gullikson, and J. C. Davis, At. Data Nucl. Data Tables **54**, 181 (1993).
[11]L. G. Parratt, Phys. Rev. **95**, 359 (1954).
[12]S. L. Johnson, P. Beaud, C. J. Milne, F. S. Krasniqi, E. S. Zijlstra, M. E. Garcia, M. Kaiser, D. Grolimund, R. Abela, and G. Ingold, Phys. Rev. Lett. **100**, 155501 (2008).
[13]S. L. Johnson, P. Beaud, E. Vorobeva, C. J. Milne, É. D. Murray, S. Fahy, and G. Ingold, Acta Crystallogr., Sect. A: Found. Crystallogr. **66**, 157 (2010).
[14]Y. M. Sheu, M. Trigo, Y. J. Chien, C. Uher, D. A. Arms, E. R. Peterson, D. A. Walko, E. C. Landahl, J. Chen, S. Ghimire, D. A. Reis, Solid State Commun. **151**, 826 (2011).
[15]E. M. Dufresne, B. Adams, D. A. Arms, M. Chollet, E. C. Landahl, Y. L. Li, D. A. Walko, and J. Wang, in *The Tenth International Conference on Synchtrotron Radiation Instrumentation*, edited by R. Garrett, I. Gentile, K. Nugent, and S. Wilkins (American Institute of Physics, Melville, NY, 2010), p. 181.
[16]D. A. Walko, D. A. Arms, and E. C. Landahl, J. Synchrotron Radiat. **15**, 612 (2008).
[17]R. M. Costescu, M. A. Wall, and D. G. Cahill, Phys. Rev. B **67**, 054302 (2003).